CROSS-FLOW TURBINE PERFORMANCE AND WAKE CHARACTERIZATION

Brian Polagye[1]
University of Washington,
NNMREC
Seattle, WA, USA

Robert Cavagnaro
University of Washington,
NNMREC
Seattle, WA, USA

Adam Niblick
Creare, Inc.
Hanover, NH, USA

Taylor Hall
Battelle Memorial Institute
Columbus, OH, USA

Jim Thomson
University of Washington,
NNMREC
Seattle, WA, USA

Alberto Aliseda
University of Washington,
NNMREC
Seattle, WA, USA

[1]Corresponding author: bpolagye@uw.edu

ABSTRACT

Helical, cross-flow turbines have a number of attractive properties for use in generating electricity from fast moving tidal, ocean, and river currents. These include low torque oscillations, inherent flow alignment in a vertical orientation, and a convenient form factor. However, the hydrodynamics of these turbines are not as well understood as for axial flow or straight-bladed, cross-flow variants. This paper presents results from simulations, laboratory experiments, and field studies of helical, cross-flow turbines with emphasis on performance, wake characteristics, and responsiveness to inflow turbulence. These results demonstrate the utility of combining numerical modeling with laboratory and field experiments and suggest a number of avenues for future study.

INTRODUCTION

Cross-flow turbines are a technology capable of generating power from swiftly moving tidal, ocean, and river currents. Close analogues to vertical axis wind turbines, cross-flow turbines have several desirable attributes relative to axial-flow (horizontal axis) turbines. Among these is a rectangular form factor that enables cross-flow turbines to achieve a high blockage ratio (i.e., ratio of turbine swept area to channel cross-sectional area) in natural and man-made channels [1]. Turbines arranged to achieve a high blockage ratio are able to exceed the Betz limit associated with unconfined flows [2], since this arrangement allows an array to draw on the potential energy in the flow.

Among the cross-flow turbine variants are straight- and helical-bladed designs. In both cases, the blades have a hydrofoil profile, but for helical blades, the profile traces out a helical sweep along the blade span [3,4,5]. If a helical turbine is designed to achieve a "full wrap" (i.e., no circumferential void space between the end of one blade and the beginning of another), then at any angular position, a point along the span of one blade will always be at the optimal angle of attack and the torque produced will be nearly constant. This overcomes the potentially damaging "stutter-start" behavior for straight-bladed cross-flow turbines. Specifically, because the entire blade of a straight-bladed rotor achieves maximum torque at one angular position, a turbine operating in a turbulent flow near its cut-in velocity can stutter between high and low torque positions, starting and stopping multiple times in a single "start-up" period [3]. In addition, a vertically-oriented cross-flow turbine allows for inherent yaw alignment without a yaw drive mechanism.

Set against these benefits are the complex hydrodynamics associated with a cross-flow geometry. In operation, the vortices shed from blades on the upstream portion of their rotation may interact with the downstream blades, as shown in Figure 1, giving rise to more complicated hydrodynamics than those of horizontal axis turbines.

To date, our research has combined numerical simulations, laboratory experiments, and field studies to better understand the hydrodynamics, power performance, and wake characteristics of helical, cross-flow turbines. These have included tests with four-bladed turbines at blade chord Reynolds numbers up to 10^5. This paper presents two aspects of that research: (1) a comparison of hydrodynamic performance obtained through
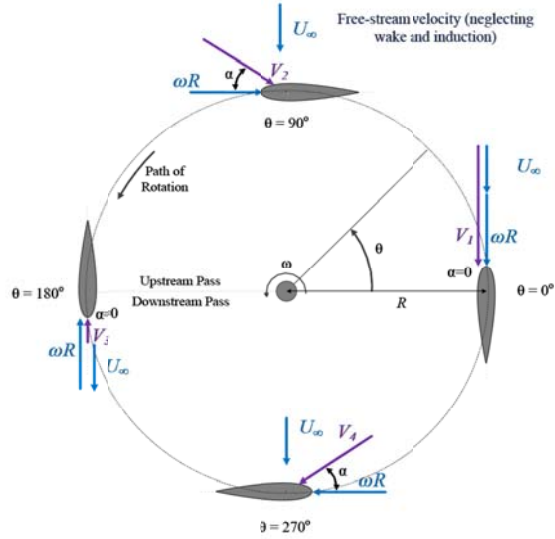
FIGURE 1. CROSS-FLOW TURBINE FLOW GEOMETRY. ADAPTED FROM [6].

numerical simulations and laboratory flume experiments of four-bladed turbines and (2) early results from field experiments, including wake characteristics and the dynamic response of a coupled turbine-generator system to inflow current variations.

METHODOLOGY

Turbine Description

The turbines used in numerical, laboratory, and field experiments are four-bladed, helical, cross-flow turbines, with parameters presented in Table 1. The solidity ratio (σ) is defined as the fraction of the turbine circumference occupied by the blades. Both three-bladed and four-bladed turbines with equivalent solidity ratios were compared in exploratory experiments [6] and the four-bladed turbine demonstrated superior performance. For this reason, subsequent numerical, laboratory, and field experiments focused on a four-bladed design. The leading edge and trailing edge of each blade are located at the same radius from the center of rotation, resulting in zero blade pitch (referenced to the half chord). The laboratory-scale turbine blades were machined from an aluminum alloy (6061-T6). The field-scale turbine blades were fabricated from a glass-fiber composite using a resin-infusion manufacturing process. The NACA 0018 profile was chosen for its well-documented hydrodynamic properties and mechanical strength.

Turbine Performance

Several parameters are used to describe turbine operation and its performance. The tip

TABLE 1. TURBINE PARAMETERS.

Parameter	Laboratory-scale turbine	Field-scale turbine
Blade profile	NACA 0018	NACA 0018
Turbine diameter (D)	17.2 cm	72.4 cm
Turbine height (H)	23.4 cm	101.3 cm
Turbine aspect ratio (H/D)	1.36	1.40
Helical pitch angle (θ)	60º	60º
Blade chord length (c)	4.05 cm	17.3 cm
Blade thickness (t)	0.73 cm	3.1 cm
Solidity ratio (σ)	0.30	0.30

speed ratio (λ) is defined as

$$\lambda = \frac{\omega R}{U_\infty} \tag{1}$$

where ω is the turbine's rotational rate, R is its radius and U_∞ is the water current velocity upstream of the turbine's hydrodynamic influence. The coefficients of dynamic torque (C_Q) and performance (C_P) are defined as

$$C_Q = \frac{\tau}{\rho U_\infty^2 R^2 H} \tag{2}$$

$$C_P = \frac{P}{\rho U_\infty^3 RH} = \frac{\tau\omega}{\rho U_\infty^3 RH} \tag{3}$$

where τ is the torque produced by the turbine, P is the power extracted from the flow, and ρ is the density of water (1000 kg/m^3 – all experiments and simulations conducted in fresh water). Neglecting induction, the relative current (U, as seen by an observer in the blade's frame of reference) is

$$U = U_\infty \left(1 + 2\lambda \cos\theta + \lambda^2\right)^{\frac{1}{2}} \tag{4}$$

where θ is the angular position of the blade, as defined in Figure 1. The blade chord Reynolds number (Re_c), defined in terms of the relative current, is given as

$$Re_c = \frac{\rho U c}{\mu} \tag{5}$$

where μ is the dynamic viscosity of water (1.002x10^{-3} Pa-s). This can lead to some ambiguity when comparing performance between experiments since the choice of velocity scale significantly affects Re_c, as shown in Figure 2. The top panel shows the ratio of Re_c calculated on the
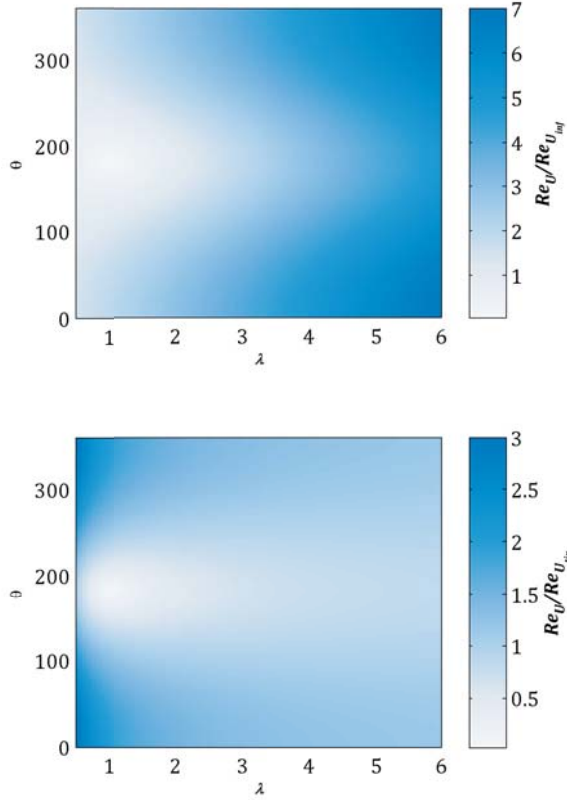
FIGURE 2. DIFFERENCE IN Re_c USING A LOCAL VERSUS FREE STREAM VELOCITY SCALE (TOP) AND LOCAL VERSUS BLADE TIP VELOCITY SCALE (BOTTOM).

basis of U compared to Re_c calculated on the basis of U_∞. For cross-flow turbines operating at $\lambda < 3$, the angular dependence dominates and the locally-defined Re_c can be an order of magnitude smaller than the free-stream Re_c. Similarly, at $\lambda > 5$, the angular dependence is negligible, but the locally-defined Re_c can be an order of magnitude larger than the free-stream Re_c. Alternatively, as shown in the lower panel, the Re_c can be defined in terms of the blade tip velocity ($U_\infty \lambda$). As shown in the lower panel of Figure 2, the angular dependence is relatively minor for $\lambda > 3$ and closely approximates the locally-defined Re_c. However, since $\lambda < 2$ for the turbines discussed in this study, the locally-defined Re_c (Equation 5) is used for clarity.

Unlike an axial flow turbine, the blades on a cross-flow turbine experience large and rapid variations in their angle of attack (angle between the blade chord line and U). The angle of attack (α) is given as

$$\alpha = \tan^{-1}\left(\frac{\sin\theta}{\lambda + \cos\theta}\right).$$
(5)

As shown in Figure 3, α can take on values that static hydrofoil theory would suggest places the
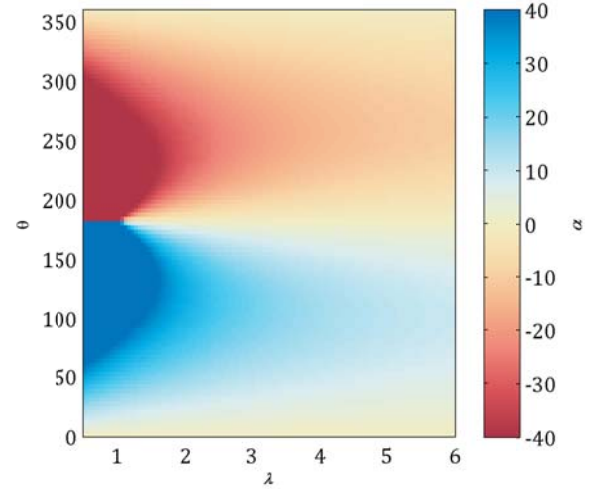
FIGURE 3. VARIATION IN ANGLE OF ATTACK AS A FUNCTION OF ANGULAR POSITION (θ) AND TIP SPEED RATIO (λ) FOR CROSS-FLOW TURBINES. COLOR SCALE SATURATES AT ±40º.

blade in deep stall. However, because of the rapid time-variation of α, the blades experience an unsteady hydrodynamic effect known as "dynamic stall" [e.g., 7], whereby the blade maintains a favorable lift to drag ratio at higher angles of attack compared to static conditions.

Equally important to the interpretation of the performance results are several characteristics of the flow environment. The blockage ratio (ε) is defined as

$$\varepsilon = A_c / 2RH.$$
(6)

where A_c is the channel cross-sectional area. The Froude number (Fr) is defined as

$$Fr = U_\infty / \sqrt{gh}$$
(7)

where g is the acceleration due to gravity (9.81 m/s²) and h is the water depth. The performance of a turbine in confined flow may significantly exceed that of a turbine in unconfined flow, depending on the turbine's induction factor, ε, and Fr [8]. To date, no universally accepted blockage corrections have been developed and care should be taken when comparing results between tests if these parameters vary. Finally, the turbulence intensity (I) is defined as

$$I = \sigma_U / \langle U \rangle.$$
(8)

where σ_U is the standard deviation of the flow velocity and $\langle U \rangle$ is the mean flow velocity. Turbulence intensity affects power production, as well as wake mixing (i.e., the wake mixes more rapidly with higher ambient I).
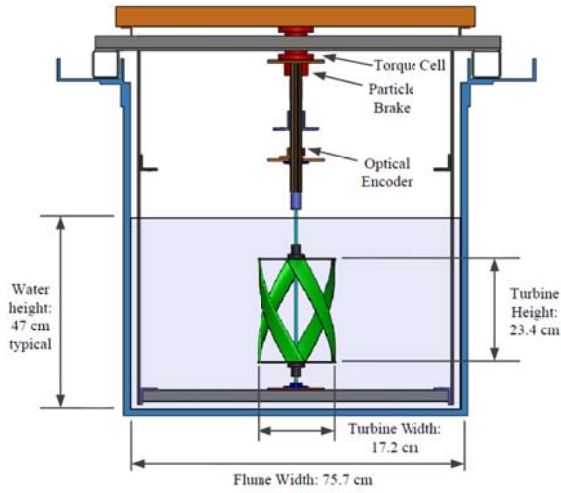
FIGURE 4. FLUME TEST CONFIGURATION.

Laboratory Experiments

Laboratory experiments were conducted in the Stevenson-Eroglu water flume at the University of Washington. The flume test section is 300 cm long and 76 cm wide. Water depth (h) was ~47 cm (3600 cm^2 cross-sectional area) and horizontal free stream velocity (U_∞) was maintained at 0.7 m/s. Accounting for the cross-sectional area of both the turbine and test rig, ε was ~19%, Fr was ~0.33, and I was ~4%.

To characterize turbine performance, a dynamometer was constructed, consisting of a particle brake, torque cell, and optical encoder mounted to a rigid frame (Figure 4). During testing, the turbine was supported at both ends by stainless steel roller bearings with its centerline at nominal mid-water depth (23 cm). Current velocity was monitored at 4Hz at a location 1.2 m (7 diameters) upstream of the turbine by an acoustic Doppler velocimeter (ADV, Nortek Vector) connected to a PC. The sampling volume for the ADV was mid-water depth (turbine horizontal and vertical centerline). At the start of each test, the turbine was allowed to reach steady state under a no-load condition and then a particle brake (Placid Industries B2-12-1) applied a constant rotational resistance. The turbine rotation rate (ω) was monitored by an optical encoder and torque was measured by a reaction torque sensor. Outputs from the torque sensor and optical encoder were recorded at 4 Hz using LabView. These values were averaged over a 30 second period to produce a low-noise representation of the power extracted by the turbine.

Numerical Simulations

The commercial Computational Fluid Dynamics (CFD) software package FLUENT (v12.0, ANSYS) was used for numerical modeling. The simulation solved the Reynolds-averaged Navier-Stokes (RANS) equations with the Shear Stress Transport (SST)-k-ω turbulence closure model on a cell-centered, control-volume space discretization. The SST-k-ω model has been used extensively as the turbulence closure for numerical modeling of wind and hydrokinetic turbines [e.g., 9], because it provides an accurate representation of the wall-bounded turbulent flow near the blade walls and the free-shear turbulence in the wake. The SIMPLE pressure-velocity coupling and second order discretization in space and time were used. A sliding mesh computational technique was used to simulate the flow field around the rotating turbine. To do so, the flow domain was divided into two zones: an inner rotating cylindrical zone which contains the fine mesh around the blades and an outer, stationary zone that defines the rest of the domain (matching that of the flume experiments). The inner zone (sliding mesh) rotates at a prescribed angular velocity and extends 1.2 turbine radii from the turbine axis and matches the height of the turbine, capped by two end plates (simulated as no-slip walls).

The spatial discretization was determined by the resolution required to capture the physics of the boundary layer on the blade surface. This depends upon the viscous length scale, which is Reynolds number dependent, and the position of the nearest grid node to the wall, expressed in term of its y^+ value, the dimensionless wall distance:

$$y^+ = u_* y / \nu .\qquad(9)$$

where u_* is the friction velocity at the wall and ν is kinematic viscosity. Comparison between numerical simulations and laboratory experiments indicated that a near-wall modeling approach with $y^+ \approx 1$ is necessary to correctly predict the boundary layer dynamics on rotating, helical blades. Further details of the simulation technique are presented in [10,12].

The numerical simulations were conducted in a domain with a cross-sectional area matching the flume experiments. However, because the test rig is not reproduced in the simulation, the blockage ratio for simulations is lower than in the experiments (ε = 11.3%). The turbulence intensity is also lower (I=1.6%) and, in a RANS simulation, the blades experience the mean, rather than turbulent flow.

Field Experiments

For field experiments, the field-scale turbine (Table 1) was mounted to the transom of an

unpowered skiff. The turbine was supported at both ends by a frame (four cylindrical members connecting a pair of cage plates). The drive shaft was connected to a 10:1 gearbox coupled to a permanent magnet 3-phase alternator (WindBlue Power). Via a DC rectifier, the alternator was connected to a load bank with ten resistive settings. During tests, a powered vessel ~100 m upstream of the skiff towed the turbine through still water at nominal velocities of 1.0, 1.5, or 2.0 m/s. The resistive bank was then cycled through its settings to develop a power-performance curve (i.e., C_P vs. λ). During tests, a data acquisition system connected to a PC monitored turbine rotational rate, voltage, and current across the load bank at a 100 Hz sampling rate. Current velocity was monitored by acoustic Doppler velocimeters (ADV, Nortek Vector) mounted 1 diameter upstream and downstream of the turbine sampling at 32 Hz.

Turbine Performance

Component efficiencies for the power train were experimentally determined in order to evaluate turbine C_P from field testing. The solid-state diode rectifier efficiency was found to be 93%, while the alternator efficiency ranged from 11% - 67% and was dependent on both shaft speed and load [11]. The efficiency of the gearbox was assumed constant at the manufacturer's specification of 95% and will be characterized in future studies. Component efficiencies were applied to the system power output to determine C_P for the rotor as

$$C_P = \frac{P_e}{\rho U_\infty^3 R H \eta_d \eta_g} \qquad (10)$$

where P_e is the electrical power dissipated by the load bank and η_d and η_g are the drivetrain (gearbox) and generator (rectifier/alternator) efficiencies defined above.

Turbine Wake

For wake characterization studies, an array of six Doppler profilers (Nortek Aquadopps) was towed behind the skiff on Dopp-cat platforms (Figure 5). The Aquadopps measured velocity at 1 Hz, using 0.5 m bins centered at the nominal 0.7 m vertical centerline of the towed turbine. During these experiments, the generator load was set to achieve maximum C_P and data was collected for five-minute intervals at near-constant velocity for multiple Dopp-cat configurations (total of 24 downstream stations).
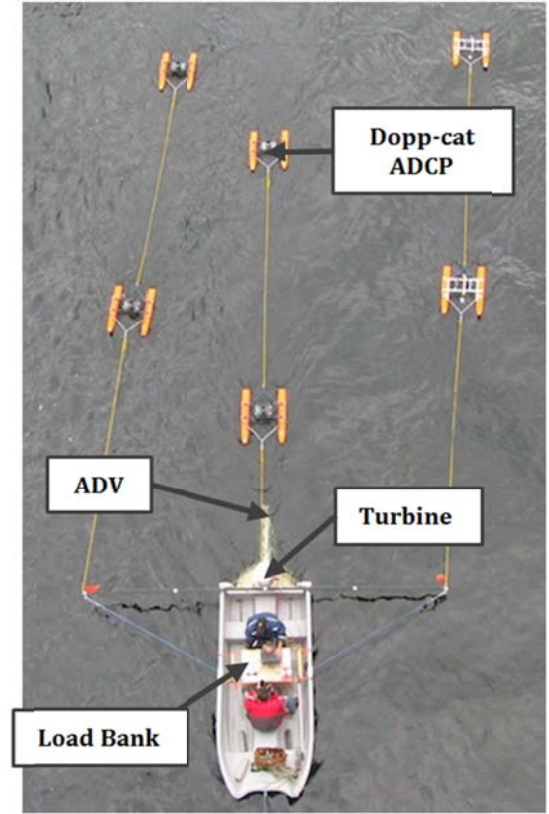

**FIGURE 5. FIELD EXPERIMENT LAYOUT FOR WAKE CHARACTERIZATION STUDIES.**

Turbine Dynamic Response

To assess the responsiveness of the turbine-generator system to variations in the inflow currents, spectra were constructed from time-series observations of the inflow kinetic power density (proportional to U_∞^3) and electrical power output. For this analysis, 45 second intervals at near-constant tow velocity were subdivided into 9-second windows with 50% overlap. Spectra for the full interval were produced by applying a fast Fourier transform to the sub-windows (with a Hamming filter) and merging the windowed spectra to achieve narrow confidence intervals.

RESULTS

Numerical Modeling and Laboratory Experiments of Turbine Performance

Numerical simulations are less expensive than laboratory experiments and are an important tool for understanding turbine hydrodynamics and optimizing design. For example, Figure 6 shows the simulated dynamic torque coefficient for each blade over a complete rotation. Angular position is referenced to the top of the first blade. Maximum torque occurs when the blade mid span is positioned at $\theta \sim 90°$. While C_Q for the individual

5
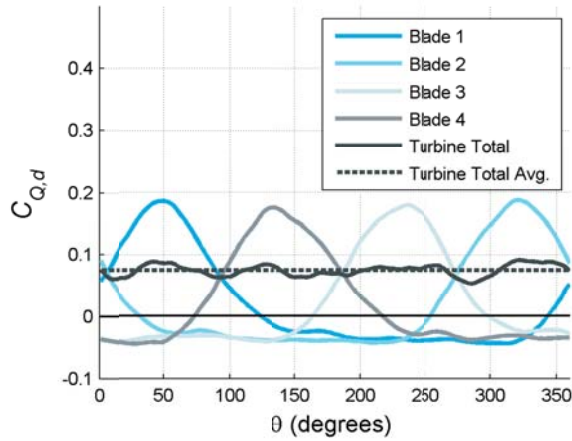
FIGURE 6. SIMULATED DYNAMIC TORQUE ($C_{Q,D}$) FOR EACH BLADE AS A FUNCTION OF ANGULAR POSITION AT λ = 1.6. θ IS REFERENCED TO THE TOP OF THE FIRST BLADE (I.E., $\theta_{\text{MID-SPAN}} = \theta + 45^{\circ}$) [12].

blades is a strong function of θ, the aggregate torque is nearly constant. This is as expected from the qualitative description of the angle of attack for a helical blade presented in the introduction, but is difficult to investigate experimentally at the level of an individual blade.

However, experimental validation is a crucial step for any numerical simulation. Figure 7 shows the comparison between C_P–λ curves for simulation and experiments at U_∞ = 0.7 m/s. As discussed in [12], there are several contributing factors to the under-prediction of C_P by simulations, including the fidelity at which the simulation predicts unsteady flow separation and differences between the experimental and simulated conditions.

First, Figure 8 shows a comparison between the experimental and simulated dynamic torque for a *single-bladed* helical, cross-flow turbine. In this case, agreement between simulations and experiments is quite good, with both showing that maximum torque occurs at similar angular position (i.e., $\theta \sim 90^{\circ}$ at mid-span on the blade). This result demonstrates the importance of dynamic stall to cross-flow turbine performance. The top panel of Figure 9 shows the static lift coefficient (C_L) for a NACA 0018 foil at Re_c = 4.6×10^4 (i.e., Re_c at blade mid-span position for maximum C_Q at λ = 1.6) over the range of α experienced by the blade. First, we note that there is some uncertainty in C_L between sources. [13] report experimental results from wind tunnel testing (blue line), while [14] report C_L over a wider range of α using a numerical panel method (black line), but did not undertake experimental validation for the NACA 0018 geometry. Regardless of the C_L source, under static conditions, flow should be separated over the majority of the blade span, as demonstrated by the

low ratio of lift to drag coefficient (C_L/C_D) shown in the bottom panel. While induction reduces the apparent free stream velocity, contracting the range of α and shifting it to lower values, for induced velocity reductions of ~20% this does not significantly alter the conclusions regarding static stall. Since this angular position is shown to generate the highest torque in both experiments and simulations, the influence of unsteady hydrodynamics is clear (i.e., dynamic stall results in favorable C_L/C_D past α corresponding to static stall). This suggests that caution should be exercised when interpreting the effect of varying Re_c on cross-flow turbine performance, since static foil performance data may be misleading.

The RANS simulations include a numerical artifact with similar consequences to dynamic stall. Namely, the simulation time step is set by the requirements for mesh compatibility between the inner, rotating mesh and outer, stationary mesh. This is prescribed by turbine rotational rate, not fidelity of flow separation from the rotating blades. Consequently, the laminar separation bubble on the foil at higher angles of attack in this quasi-steady simulation "lags" the steady-state result. Qualitatively, the performance effect is similar to dynamic stall, but is a combination of the time lag and tendency for RANS simulations to over-estimate the angle of attack at which flow separation occurs. We hypothesize that the differences between experimental and simulated C_P-λ curves (Figure 7) are primarily caused by an overall underestimation of dynamic stall by the RANS simulations. This is consistent with the good agreement between experiments and simulations at higher λ for the single-bladed turbine (Figure 8), since the angle of attack variation is decreases at higher λ (Figure 3). Consequently, dynamic stall should be less important at higher λ.

Second, the simulations are conducted at a blockage ratio of 11.3%, while the experiments are conducted at a blockage ratio of 18.7%. While the simulations do not include a free surface, the rigid lid allows static pressure to vary upstream and downstream of the turbine in the same manner as a free-surface elevation change. While no blockage corrections have been applied to experimental or simulation results, C_P has been shown to increase with ε [8]. We hypothesize that this effect is secondary to dynamic stall considerations since higher blockage ratios should also result in peak C_P shifting to higher λ, whereas peak C_P occurs at approximately the same λ in simulations and experiments.

These results suggest that numerical simulations are a useful tool for qualitative analysis of performance trade-offs across a wide range of geometric and operating conditions in the
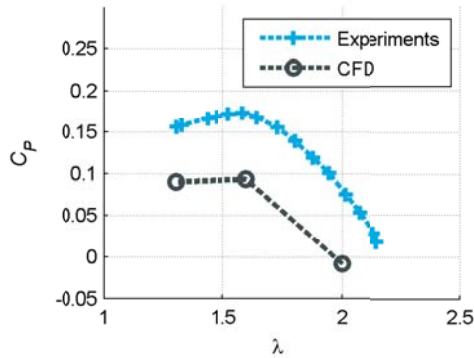
FIGURE 7. COMPARISON BETWEEN EXPERIMENTAL AND SIMULATED COEFFICIENT OF PERFORMANCE (C_P) FOR A FOUR-BLADED TURBINE AT U_∞ = 0.7 m/s [12].
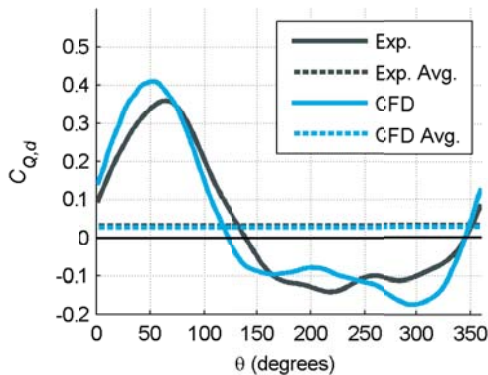

FIGURE 8. COMPARISON BETWEEN EXPERIMENTAL AND SIMULATED DYNAMIC TORQUE COEFFICIENT FOR A SINGLE-BLADED TURBINE AT λ = 3.2 AND U_∞ = 0.7 m/s. θ IS REFERENCED TO THE TOP OF THE BLADE (I.E., $\theta_{\text{MID-SPAN}} = \theta + 45^\circ$) [12].

design phase for helical, cross-flow turbines. However, experiments play a key role in quantitative performance analysis of prototypes and in validating numerical simulations.

Field Experiments

Turbine Performance

C_P versus λ for a 1.5 m/s nominal tow velocity is shown in Figure 10. Re_c at peak C_P varies from 7.9×10^4 – 4.8×10^5 over a single rotation, ε is ~0%, Fr is ~0, and I is ~4%. Re_c is approximately an order of magnitude greater than for the laboratory-scale turbine. Peak performance is observed between λ of 1 and 2 for tow velocities between 1-2 m/s, in agreement with laboratory and numerical results. However, limitations in achieving high flow speeds in the laboratory experiments (resulting in operating in a lower regime of Reynolds number) and the effects of blockage inhibit direct comparisons of performance data between field studies and laboratory experiments [11].
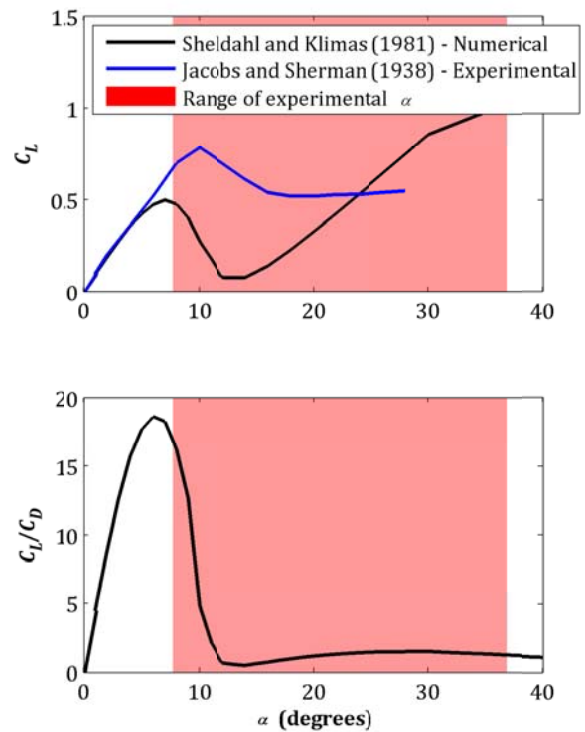

FIGURE 9. (TOP) STATIC LIFT COEFFICIENT AND (BOTTOM) RATIO OF STATIC LIFT TO STATIC DRAG COEFFICIENT FOR A NACA0018 FOIL AT Re_C = 4.6×10^4. VALUES FROM [13] AND [14] ARE INTERPOLATED FROM REPORTED RANGE OF Re_C.
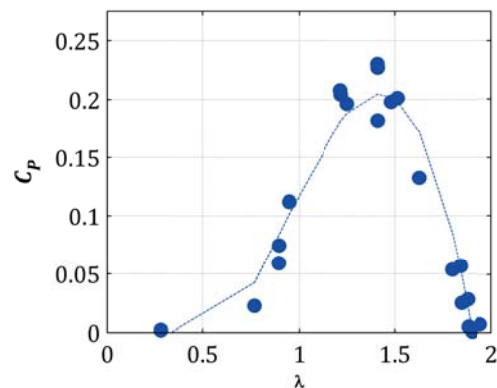

FIGURE 10. C_P AS A FUNCTION OF λ FOR FIELD-SCALE TESTING AT 1.5 m/s NOMINAL TOW VELOCITY.

Preliminary analysis suggests that the reported peak C_P values for field experiments under these conditions have an uncertainty (standard deviation of measurements and sensor accuracy) on the order of 5% of the value shown in Figure 10. This turbine's performance is in general agreement with previous studies of high-solidity, helical, cross-flow turbines [4]. Lower solidity helical cross-flow turbines [5] and straight bladed cross-flow turbines [4,15] both demonstrate higher performance coefficients, at the cost of reduced starting torque.
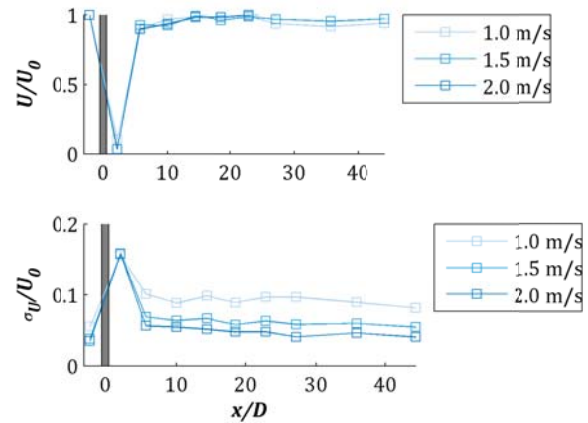
Turbine Wake

The structure of the wake downstream of a hydrokinetic turbine is an important consideration for array design, particularly for densely packed arrays attempting to exploit the performance benefits of high blockage ratios. The velocity deficit along the wake centerline observed during field experiments is shown in Figure 11 for tow velocities of 1.0, 1.5, and 2.0 m/s. Notably, directly downstream of the turbine (e.g., 1 diameter), the velocity is near-zero, indicating a strong recirculation zone. Beyond this, the wake recovers to free-stream values within 20 diameters. This is consistent with wake observations in flume experiments. The observed wake is likely more persistent than would be observed for a realistic deployment, since in both the laboratory and field experiments there is little vertical shear and low ambient turbulence (both of which are important mechanisms that promote the mixing of the wake with the free stream).

Along-channel velocity fluctuations in the wake are consistent with the observed spectrum of turbulent kinetic energy (TKE) in the wake, which indicate higher relative TKE production at lower free-stream velocity (Figure 12). As shown in Figure 13, the upstream spectra are much flatter than the spectra observed at tidal energy sites [16]. However, the downstream spectra display a classical $f^{-5/3}$ dependence associated with the decay of turbulent eddies shed by the turbine blades.

Turbine Dynamic Response

The dynamic response of the combined turbine-generator system is of interest for the design of control systems intended to maximize power output and minimize structural loads. Figure 14 shows the input and output power spectra for 1.5 m/s tow velocity at maximum C_P. For reference, the frequency scale associated with the turbine height is ~1.6 Hz. At frequencies lower than 1.6 Hz, the power output closely tracks the spectral content of the input power. The transfer function (Figure 15) for the system shows power output response peaks at 1 Hz before substantially dropping off at higher frequencies. This is consistent with the turbine length scales (i.e., turbulence at length scales smaller than the turbine characteristic dimensions of diameter and height will affect performance to a lesser degree than an "engulfing gust").

CONCLUSIONS

These studies of helical cross-flow, turbines have increased the understanding of the hydrodynamics influencing turbine performance, the structure of the turbine wake, and turbine

FIGURE 11. MEAN WAKE VELOCITY (TOP) AND STANDARD DEVIATION OF WAKE VELOCITY (BOTTOM) NON-DIMENSIONALIZED BY UPSTREAM VELOCITY (U_0) ALONG THE WAKE CENTERLINE. GREY SHADING DENOTES TURBINE POSITION.

response to variations in inflow velocity. Results demonstrate the utility of combining numerical modeling with laboratory and field experiments and suggest a number of avenues for future study. First, given the importance of accurately predicting dynamic stall, further numerical studies could be undertaken to more rigorously define the requirements for resolving dynamic stall behavior. Second, in order to enable direct comparisons between laboratory and field experiments, blockage corrections should be developed. Likewise, such comparisons would be enhanced through a more thorough understanding of how dynamic stall varies with blade chord Reynolds number. Finally, the field studies suggest a number of interesting possibilities for turbine control to track turbulent perturbations to enhance power generation or reject them to decrease structural loads.
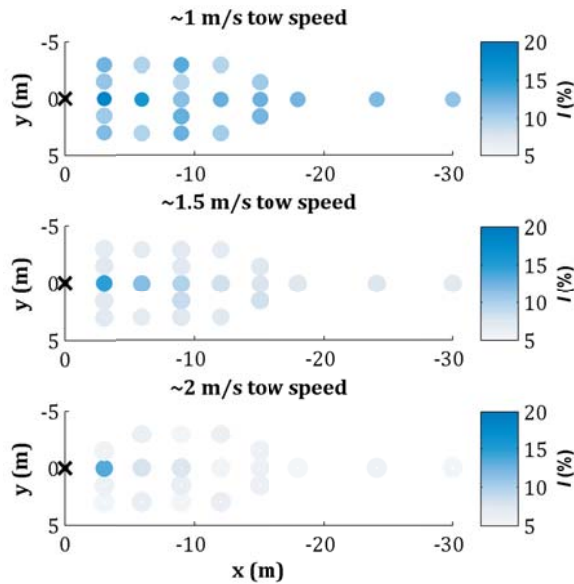
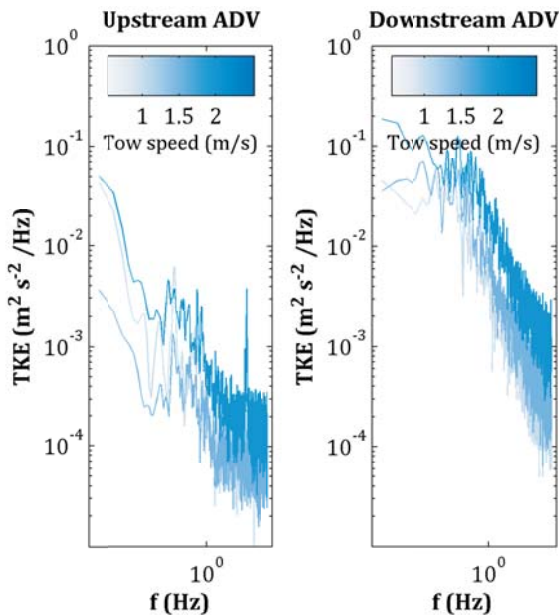**FIGURE 12. TURBULENCE INTENSITY (*I*) AS A FUNCTION OF TOW SPEED.**

FIGURE 13. UPSTREAM AND DOWNSTREAM TKE SPECTRA.

REFERENCES

1 Salter, S.H., 2012 "Are nearly all tidal stream turbine designs wrong?," *International Conference on Ocean Energy*, Dublin, Ireland, October 17-19.

2 Garrett, C. and Cummins, P., 2007, "The efficiency of a turbine in a tidal channel," *Journal of Fluid Mechanics*, **588**, 243-251.

3 Gorlov, A., 1998, "Helical turbines for the Gulf Stream: conceptual approach to design of a large-scale floating power farm," *Marine Technology*, **35**(3): 175-182.
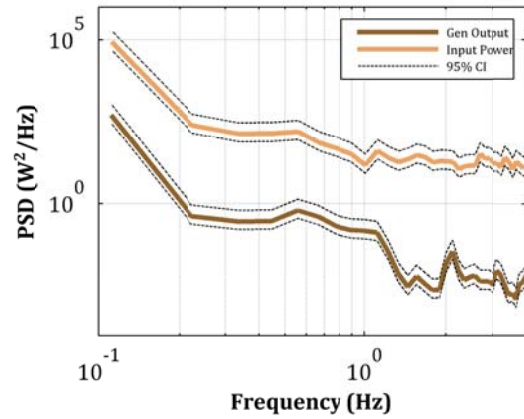
FIGURE 14. SPECTRA FOR INFLOW POWER AND OUTPUT GENERATION AT 1.5 m/s TOW VELOCITY AND MAXIMUM *C_P*. BLACK LINES DENOTE 95% CONFIDENCE INTERVALS FOR EACH SPECTRUM.
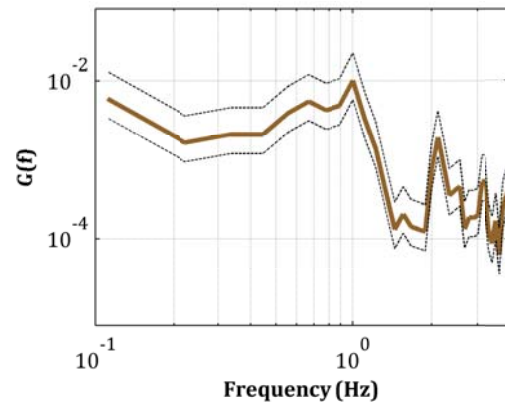

FIGURE 15. TRANSFER FUNCTION FOR OUTPUT POWER RESPONSE WITH INFLOW POWER AS EXCITATION. BLACK LINES DENOTE 95% CONFIDENCE INTERVAL.

4 Shiono, M., Suzuki, K. and Kiho S., 2002, "Output characteristics of Darrieus water turbine with helical blades for tidal current generations," *Proceedings of the Twelfth (2002) International Offshore and Polar Engineering Conference* (pp. 859-864). Kitakyushu, Japan.

5 Bachant, P., and Wosnik, M., 2011, "Experimental investigation of helical cross-flow axis hydrokinetic turbines, including effects of waves and turbulence," *Proceedings of the ASME-JSME-KSME 2011 Joint Fluids Engineering Conference*, Hamamatsu, Shizuoka, Japan.

6 Niblick, A.L., 2012, "Experimental and analytical study of helical cross-flow turbines for a tidal micropower generation system," Masters thesis, University of Washington, Seattle, WA.

7 Masson, C., Leclerc, C., and Paraschivoiu, I. 1998, "Appropriate dynamic-stall models for performance predictions of VAWTs with NLF blades," *International Journal of Rotating Machinery*, **4**(2), 129-139.

8 Whelan, J.I., Graham, J.M.R., and Peiro, J., 2009, "A free-surface and blockage correction for tidal turbines," *Journal of Fluid Mechanics*, **624**(1), pp. 281-291.

9 Castelli, M.R. and Benini, E., 2012, "Effect of blade inclination angle on a Darrieus wind turbine," *Journal of Turbomachinery-Transactions of the ASME*, **134**(3).

10 Hall, T., 2012, "Numerical simulation of a cross flow marine hydrokinetic turbine," Master's thesis, University of Washington, Seattle, WA.

11 Polagye, B., Cavagnaro, R.J., and Niblick, A., 2013, "Micropower from tidal turbines," *Proceedings of the ASME 2013 Fluids Engineering Division Summer Meeting.*

12 Hall, T., Niblick, A., Polagye, B., and Aliseda, A., *Submitted*, "An experimental and numerical study of the hydrodynamic performance of a helical, cross-flow marine hydrokinetic turbine." Submitted to *Renewable Energy*.

13 Jacobs, E.N., and Sherman, A., 1937, "Airfoil section characteristics as affected by variations of the Reynolds number," Report No. 586, National Advisory Committee for Aeronautics.

14 Sheldahl, R. E. and Klimas, P. C., 1981, "Aerodynamic characteristics of seven airfoil sections through 180 degrees angle of attack for use in aerodynamic analysis of vertical axis wind turbines," SAND80-2114, March 1981, Sandia National Laboratories, Albuquerque, New Mexico.

15 Li, Y. and Calisal, S.M., 2010, "A Discrete Vortex Method for Simulating a Stand-Alone Tidal-Current Turbine: Modeling and Validation." *Journal of Offshore Mechanics and Arctic Engineering. Transactions of the ASME*, **132**(3).

16 Thomson, J., Polagye, B., Durgesh, V., and Richmond, M., 2012, "Measurements of turbulence at two tidal energy sites in Puget Sound, WA (USA)," *Journal of Oceanic Engineering*, **37**(3)